



**Rational Design of BIAN Based Multi-functional Additive for Higher Durability and Performance of LiMn<sub>1/3</sub>Ni<sub>1/3</sub>Co<sub>1/3</sub>O<sub>2</sub> Cathodes**

Journal:	<i>Molecular Systems Design &amp; Engineering</i>
Manuscript ID	ME-ART-04-2019-000046.R1
Article Type:	Paper
Date Submitted by the Author:	10-May-2019
Complete List of Authors:	Patnaik, Sai Gourang; Japan Advanced Institute of Science and Technology (JAIST), School of Materials Science Vedarajan, Raman; International Advanced Research Centre for Powder Metallurgy and New Materials, Centre for Fuel Cell Technology Matsumi, Noriyoshi; Japan Advanced Institute of Science and Technology (JAIST), School of Materials Science

**Design, System, Application****Rational Design of BIAN Based Multi-functional Additive for Higher Durability and Performance of  $\text{LiMn}_{1/3}\text{Ni}_{1/3}\text{Co}_{1/3}\text{O}_2$  Cathodes**

*Sai Gourang Patnaik<sup>□</sup>, Raman Vedarajan<sup>‡</sup> and Noriyoshi Matsumi<sup>\*</sup>*

<sup>\*</sup>School of Materials Science, Japan Advanced Institute of Science and Technology (JAIST), 1-1 Asahidai, Nomi, Ishikawa, 923-1292, Japan. E-mail: [matsumi@jaist.ac.jp](mailto:matsumi@jaist.ac.jp)

Oxidation of carbonate based electrolytes in high voltage cathodes is necessary to a limited extent for the formation of a solid electrolyte interface (SEI) which largely determines the future performance of the battery. This is particularly important in  $\text{LiMn}_{1/3}\text{Ni}_{1/3}\text{Co}_{1/3}\text{O}_2$  cathodes, which show stable cycling up to 4.8 V. But the stability of the commercial electrolyte is only up to ~3.8 V. A huge part of successful strategies relies on the utilization of electrolyte additives that oxidize before the onset of oxidation of actual electrolyte, thereby preventing further electrolyte degradation.

Herein, Bisiminoacenaphthene based diamine additive is introduced serving multiple objectives as an electrolyte additive at very low weight fraction. Appropriate design of the functional groups gives optimum HOMO (Highest occupied molecular orbitals) for preventing irreversible electrolyte oxidation. The amine functional group aids in neutralizing in-situ generated hydrofluoric acid (HF) and electropolymerises in an intrinsically oxidizing environment. The imine moiety, well known for their coordinating ability, can help in adherence of the polymerized film on to the active materials. These design principles at the molecular level reflect in the final device performance relating individually to cycling stability, lower electrolyte oxidation, robust SEI, lower impedance rise and better morphological characteristics.

(197 words)

**Rational Design of BIAN Based Multi-functional Additive  
for Higher Durability and Performance of  
 $\text{LiMn}_{1/3}\text{Ni}_{1/3}\text{Co}_{1/3}\text{O}_2$  Cathodes**

*Sai Gourang Patnaik<sup>□</sup>, Raman Vedarajan<sup>‡</sup> and Noriyoshi Matsumi<sup>\*</sup>*

\*School of Materials Science, Japan Advanced Institute of Science and Technology

(JAIST), 1-1 Asahidai, Nomi, Ishikawa, 923-1292, Japan. E-mail:

[matsumi@jaist.ac.jp](mailto:matsumi@jaist.ac.jp)

**Abstract**

The theoretical capacity and potential limit of modern Li-ion batteries is hugely determined the type of the cathode material utilized. With the dawn of 5V cathode materials, the major problem severely affecting wide scale commercial utilization is the stability of the commercially available  $\text{LiPF}_6$  in carbonates as electrolytes. Problems like electrolyte oxidation at high potential, formation of surface reaction layer, and steadily increasing impedance upon storage are yet to be solved to realize their wide scale application. In this regard, novel bisiminoacenaphthene based functional polymerizable diamine, which was found to be serving multiple purposes as an electrolyte additive is reported. Apart from reducing irreversible electrolyte oxidation at high potential, BIAN based additives also aided in neutralizing the in-situ generated hydrofluoric acid (HF). The diimine unit can help adhere the electropolymerized product on to the surface of the metal oxides and provide a robust interface, leading to performance enhancement.

Keywords: Electrolyte additive, MNC cathodes, Electropolymerisation, Li-ion battery

## 1. Introduction

High energy Li ion batteries (LiBs) have seen a sharp growth in commercial domain as well as research arena, owing to their utility in electric vehicles (EVs), hybrid storage systems and plethora of other applications. However, to scale up their utilisation from only portable electronics to high energy demanding applications like EVs, it is necessary to develop and study new cathode materials which can provide higher operating voltage and power density<sup>1</sup>. Currently, Ni-Mn-Co based mixed oxides (MNC) have been studied extensively for such applications because of their higher power density, specific capacity and high operating potential (up to 4.5 V Vs Li/Li<sup>+</sup>)<sup>2</sup>. However, the major drawback that is still to be solved is the issue of electrolyte oxidation and associated issue of structural stability of the electrode during high voltage operation<sup>3,4</sup>. Traditional Li salts in low molecular weight carbonate based solvents have long been utilised owing to their favourable properties and still dominate the commercial domain. But the relatively high lying HOMO (Highest occupied molecular orbital) of the carbonate based electrolytes makes them susceptible to easy oxidation at higher potentials. At high potentials (>4.0), transition metal based positive electrodes acts as catalytic centres for decomposition of salts like LiPF<sub>6</sub> in carbonate based electrolytes as  $\text{LiPF}_6 \rightarrow \text{LiF} + \text{PF}_5$ <sup>5,6</sup>. Trace amount of water can then trigger further side reactions as  $\text{PF}_5 + \text{H}_2\text{O} \rightarrow \text{PF}_3\text{O} + 2\text{HF}$ , forming HF. The generated HF further leads to multiple problems like dissolution of CEI (cathode electrolyte interface), corrosion of the electrode surface etc., thus increasing the overall cell impedance<sup>3</sup>. In a similar manner, the formed phosphorus oxides can also get deposited on the surface of the electrodes leading to impedance rise. Apart, from electrolyte oxidation, it is also well known that the surface of the positive electrode material itself undergoes structural changes upon contact with LiPF<sub>6</sub> in EC:DEC, forming a surface reconstruction layer, which leads to impedance rise<sup>7</sup>. Till date, numerous additives have been designed and utilised with an aim to mitigate each of the above mentioned problems.

Additives normally focus on either enhancing the CEI, scavenging the insitu generated HF or on increasing the oxidative potential of the carbonate based electrolytes<sup>8-12</sup>. Majority of additives in this category are either fluorine or imino containing organic materials. For example, Lee et.al<sup>10</sup> utilised self-oxidative polymerisation of dopamine to obtain polydopamine layer on cathode surface for protection against oxidative decomposition of electrolyte components. Zhou et.al<sup>13</sup> reported N,N-diethylamino trimethylsilane based bifunctional additive for H<sub>2</sub>O/HF scavenging and robust interface formation. Similar enhancements in interface were also reported by Huang et.al<sup>14</sup> using 4-(Trifluoromethyl)-Benzonitrile as the additive for MNC based cathodes. Whereas, to mitigate the problem of maintaining structural stability, various techniques like coating with ZnO, Al<sub>2</sub>O<sub>3</sub> or AlF etc. have also been developed<sup>15-17</sup>. However, there have not been many reports on additives that simultaneously address multiple issues faced by MNC based cathode materials.

Hence, in this scenario, there is a strong need for additives that can serve multiple functions during battery cycling at high voltage. Here, we introduce bisiminoacenaphthequinone (BIAN) based novel electropolymerisable diamine having a general framework of  $\pi$ -s-p ( $\pi$ -spacer-polymerisable group) as ligand inspired electrolyte additive for enhanced performance and storage properties of cathode materials (Scheme 1). BIAN based ligands have been studied extensively as ligands for transition metal atoms and utilised in catalysis owing to their e<sup>-</sup> reservoir nature<sup>18-24</sup>. The diamine was designed using DFT studies to have appropriate HOMO and synthesised via simple Schiff's base condensation reaction from readily available commercial reagents. We also show ex-situ electropolymerisation of the synthesised diamine as a proof of concept of in-situ polymerisation. The effect of the additive was then characterised by various electrochemical and physical techniques. The evolution of the interface of the electrode with the additive was also studied by dynamic electrochemical impedance spectroscopy (EIS). The interesting results indicated that the highly reactive

diamine additive not only enhanced long term performance, but also prevented impedance rise upon storage.

## 2. Results and discussions

### 2.1. Theoretical studies

Even though most carbonate based electrolytes are theoretically stable up to 6 V vs Li/Li<sup>+</sup> <sup>25</sup>, the metal centres on cathode surface act as catalytic centres, leading to their oxidation at lower potentials. This comes from their high HOMO levels, which makes them susceptible to oxidative degradation at higher potential<sup>26</sup>. To understand the energy levels of BIANODA (*acenaphthylene-1,2-diylidene-bis(4-(4-aminophenoxy)aniline)*) with respect to carbonate based electrolytes, we performed DFT calculations using Gaussian 09 application. Figure 1 shows the DFT optimised structure of BIANODA and summarises the comparison of energy levels of various carbonate based electrolytes with BIANODA. Theoretical calculations thus suggest that, due to higher HOMO levels compared to any of the carbonate based electrolytes, BIANODA should undergo oxidative degradation before actual electrolyte, contributing to formation of a cathode electrolyte interface (CEI). Also, the diimine entity in BIANODA should also help the additive molecules to have coordinative interaction with metal atoms on the cathode surface, aiding in CEI formation on application of potential.

### 2.2. Cyclic voltammetry studies

To evaluate the electrochemical characteristics of the additive, we performed cyclic voltammetry studies. Figure S1 shows the comparison of first cycle of CV profiles of cathodic half cells with and without BIANODA. As can be seen clearly, in case of BIANODA, the onset of oxidation starts at ~3.80 V vs Li/Li<sup>+</sup> compared to oxidation at 4.15 V vs Li/Li<sup>+</sup> for the control cell. This shift in onset potential thus correlates well to our initial assumption from DFT studies, that BIANODA will undergo oxidative degradation before the oxidation of carbonate based electrolytes. Further observation of subsequent CV cycles for

both the cases revealed interesting information. Figure 2 shows comparison of four CV cycles with and without BIANODA respectively. The CV profiles for both the cases show the usual two pairs of characteristic redox peaks corresponding to  $\text{Ni}^{2+}/\text{Ni}^{4+}$  and  $\text{Co}^{3+}/\text{Co}^{4+}$  respectively, when cycled up to 5V vs Li<sup>16,27,28</sup>. On careful observation, it was noticed that after the first cycle, the current values remained almost in the same range for the subsequent cycles in the cell without any additive, indicating continuous electrolyte degradation at higher potentials. However, in case of BIANODA, the current in oxidation cycle drastically decreased to almost zero after second cycle, indicating that electrolyte degradation decreased considerably after first cycle.

This may be attributed to the robust BIANODA derived CEI, which partially shields the cathode surface from direct exposure to the electrolyte.

### 2.3. Charge-discharge measurements

Figure 3 shows comparison of discharging capacity retention of cells with and without BIANODA at 1C rate for two different potential ranges. For this study, the cells were first cycled at C/20 for two cycles for CEI formation followed by long cycling at 1C. In the first case, i.e. cycling up to 4.5V, the reversible capacity retention of the cell with BIANODA is evidently higher than that of the case without additive. In case of further high voltage cycling up to 4.8V also, the performance of the cell with BIANODA was better than that without additive. More interestingly, in case of cycling up to 4.8V, side reactions becomes severe in cell without additive, shown by irregularities in the discharging capacity as well as coulombic efficiency plots. However, in case of the cells with additive, the CEI, comprising of the electropolymerised BIANODA helps in curbing rapid electrolyte degradation and hence side reactions. Apart from electrolyte oxidation, the diimine group in BIANODA can also be expected to help in preventing leaching of metal ions into the electrolyte. We also performed rate studies with and without BIANODA, with five cycles at each rate, cycled up to 4.5V.

This also followed the same trend with better capacity retention with BIANODA (Figure 4). However, it should be noted here that the cell capacities mentioned are with respect to the entire weight of the cathode material including the binder and carbon additives and not active material alone and hence relatively lower specific capacity. This is because of nondisclosure of exact amount of active materials utilised by the electrode vendor due to copyright issues.

We also evaluated the effect of increasing the concentration of BIAONDA (Figure S2). The behaviour was similar up to 4 mg/ml of additive and decrease in discharge capacity retention was observed at 6 mg/ml concentration. This might be because of excess additive hindering  $\text{Li}^+$  access to the host material.

#### 2.4. Impedance spectroscopy

To further understand the CEI formed after cycling, we performed dynamic electrochemical impedance spectroscopy studies. Unlike classic electrochemical impedance spectroscopy (EIS), dynamic EIS measures the impedance response of lithium-ion batteries during charge/discharge at different potential steps, rather than taking impedance at one particular state of charge (SOC) in EIS<sup>29–35</sup>. This is particularly helpful to study the evolution of the CEI at different potentials during actual charge/discharge conditions. We have previously applied dynamic EIS to study BIAN based binders for anode, obtaining very useful information about interface evolution<sup>36</sup>. Hence, we performed dynamic EIS studies on cathodic half cells in this study, obtaining impedance responses at different potential steps between 3.0–4.5 V. Figure 5 show the dynamic EIS profiles of cathodic half cells with and without BIANODA respectively. In case of cell without additive, there is only one prominent semicircle in the high frequency region, corresponding to  $R_{\text{CEI}}$ , which remains uniform throughout the potential range. However, in case of the cell with BIANODA, one can observe another additional semicircle in the high potential region i.e from 3.60 V to 4.50 V, thereby indicating a

different interfacial process at higher potentials. We further performed equivalent circuit (Figure 6 (a)) fitting to have quantitative measure of impedance at different potentials. The choice of circuit for each case and associated components are described in Figure S3 and Figure S4<sup>37</sup>. Circuiting fitting analysis showed that the  $R_{CEI}$  was almost 25  $\Omega$  less in case of additive as compared to the case without the additive (Figure 6 (b)). Such lower impedance in case of additive is ascribed to the formation of a better interface as well as the ability of the diamine to neutralise the generated HF, which might lead to further side reactions.

### 2.5. *Morphology and impedance upon storage*

One of the major problems with MNC based cathodes in carbonate based electrolytes with  $\text{LiPF}_6$  is their stability on storage. Doeff et.al<sup>7</sup> showed the formation of surface reconstruction layer on MNC cathodes on storage in carbonate based electrolytes in  $\text{LiPF}_6$ . They showed that, the formation of a surface reaction layer is most probably responsible for impedance build up and capacity fading during high voltage cycling. They found that the effects of exposing the electrodes to the electrolytes are similar to that of cycling, although to a lesser extent. Hence, to check if addition of small amount of basic diamine can help prevent the formation of surface reaction layer, we stored the electrodes in commercial electrolyte solutions with and without additive for seven days in argon atmosphere. Figure 7 shows the comparison of SEM images of the electrodes at different magnifications after storing them in electrolytes with and without BIANODA. The morphology of the pristine electrode surface shows micrometre size spherical particles of MNC with uniformly distributed matrix of conductive additives. The micrometre size particles are further composed of smaller bead like structures. After storing the particles in electrolyte without additive, we could see that the primary structure has disintegrated into smaller fragments with the bead like substructures not clear anymore. The entire matrix seems to be covered with an opaque turbid layer (mostly the surface reaction layer). On the contrary, in case of the electrode stored in electrolyte

BIANODA, we can see that the primary structure has not been fully disintegrated and the bead like substructures are more clearly visible as compared to the case without the additive. This shows that, in case of electrodes stored in electrolyte with BIANODA, the formation of the surface reaction layer is slower as compared to the case without additives. This is further evident in impedance responses of cathodic half-cells (at OCV/ 0% SOC) upon storage. Figure 8 shows the rise in impedance upon storing the fabricated half cells with and without additives respectively. It's clearly evident that the impedance continues to rise drastically in cell without additive as compared to cell with BIANODA.

### 2.6. XPS studies

To further supplement our understanding of the interface from DEIS measurements, XPS measurements were performed on the electrodes. As widely known, there are two dominant processes that occur during cycling of the cathodes. Firstly, the electrolyte oxidation products form a passivation layer similar to CEI of anodes. Second, a surface reconstruction layer is formed by the diffusion of the metal ions on to the surface during repeated lithiation-delithiation process. Hence to gain in-depth CEI profiling, we performed XPS measurements on the pristine cathode, cathode cycled without the additive for 100 cycles and cathode cycled with 2mg/ml BIANODA for 100 cycles.

The broad scan XPS of the electrode surface under different conditions are shown in Figure S5. The pristine electrode surface lacks signal corresponding to phosphorus as no electrolyte oxidation products is present. In case of cycled cathodes, both with and without additives, the signals corresponding to Mn 2p and Co 2p are not conspicuous, mostly because of screening by electrolyte oxidation products. But, the Ni 2p peaks are clearly visible even after cycling.

The C 1s spectra for the cathodes are shown in Figure S6. The pristine uncycled cathode spectra has three major components, C-C (284.6 eV), C-O (286.2 eV), and CF<sub>2</sub> (~291 eV). There is also a suppressed C=O (288.3 eV). This can be due to formation of surface films

from reaction of  $\text{CO}_2$  with moisture, leading to formation of  $\text{Li}_2\text{CO}_3$ . The cycled cathodes on the other hand show very prominent  $\text{C}=\text{O}$  ( $\sim 288.3$  eV) peaks corresponding to the different oxidised carbonates from electrolyte oxidation on the surface. One other important feature is the relatively suppressed  $\text{CF}_2$  ( $\sim 291$  eV) peak in the cycled cathodes, which can be because of two reasons. Firstly, the peak would have been masked under the surface film, or secondly, the binder itself undergoes some kind of degradation.

Comparison of O 1s (Figure 9) spectra show interesting trend. In case of pristine cathodes, the lattice oxygen peak of cathodes (529.6 eV) is prominent and the second peak at 532.5 eV corresponding to  $-\text{OH}$  and carbonates appears as a broad peak. The lattice oxygen peak, which is totally masked in case of the cathodes cycled without additive, are prominent in the case of the cathode with additive. This can be because of relative less oxidation of the electrolyte due to masking of the metal centres by the additive.

Similarly, the comparison of P 2p (Figure 10) spectra indicates similar conclusion. The P-F linkage appears at 136.5 eV whereas the P-O/P=O linkages appear at around 133.2 eV. Figure 13 shows the comparison of contributions to P 2p for electrodes cycled with and without additives respectively. In case of cathodes cycled without additives, the P-F linkages are redundant where as in case of cathodes cycled with additives, the P-F linkage is quite clear. This implied that in case of cathodes without additives, most of P-F bond are converted into different P-O linkages. But in case of cathodes cycled with additives, comparatively more P-F linkages stay intact.

The F 1s (Figure 11) spectrum of pristine cathode surface shows a single peak at 688.6 eV (Figure 11 (a)) corresponding to C-F linkage of PVdF. In cycled cathodes, this peak is hidden below the thick surface film. The new F 1s peak in cycled electrodes are corresponding to P-F linkage (687.5 eV) and due to formation of LiF ( $\sim 685$  eV). In case of cathodes cycled

without additives, the contributions corresponding to P-F linkages is significantly less (Figure 11 (b)) as compared to cathode surface with additives (Figure 11 (c)). This is again in similar lines to our previous conclusions, indicating electrolyte degradation to a lesser extent in case of cathodes cycled with additives.

### 2.7. *Electropolymerisation of BIANODA*

However, XPS does not provide any information about the fate of BIANODA itself (as no clear peak corresponding to N 1s). Hence, to get more information about the fate of the diamine in the highly oxidising environment, we performed ex-situ oxidative electropolymerisation of BIANODA. It is well known that almost all diamines undergo irreversible electro oxidation<sup>38-40</sup>. However, it is extremely difficult to mimic the conditions under cathodic environment and then characterise the obtained material. Hence, we performed oxidation of BIANODA in 0.1M LiClO<sub>4</sub> in acetonitrile and tried to study the obtained product, which most probably will be similar to the products obtained during real cycling in the highly oxidising cathodic environment. Figure S7 shows the cyclic voltammograms of electropolymerisation of BIANODA. The constant increase in current with cycling indicated polymerisation of the diamine, which gradually settles down in the bottom of the vessel. Figure S8 shows the digital photographs of electropolymerisation of BIANODA during different number of scans in cyclic voltammetry. After 50 cycles, the precipitate was collected from the bottom of beaker cell, dried and used for characterisation. Figure S9 shows the <sup>1</sup>H NMR of the obtained product and Figure S10 shows the IR spectra of the product. The probable structure of the polymer that was ascertained from characterisation and its energy optimised structure are shown in Figure S11. The possible mechanism of electropolymerisation is shown in Figure 12. Figure 13 and Figure 14 show the sites for HF neutralisation and possible mechanism of Li<sup>+</sup> ion conduction respectively.

### 3. Conclusion

We report design, synthesis, and application of novel electropolymerisable diamine (BIANODA) as a cathode additive for conventional electrolytes in LiB's. The additive showed multiple functionalities like enhanced capacity retention upon cycling, lower impedance rise on storage and better retention of surface morphology compared to the case without additives, which is contrary to previous reports which focus on only a specific problem faced by high voltage cathodes (Figure S9). The enhancing effect of the additive was studied by electrochemical methods, computational tools and by physical methods, providing useful insights on their functioning. This study thus opens up a new class of oxidizable Lewis base type additives with promising results and suitability for incorporation into the current manufacturing stream.

### 4. Experimental methods

#### 4.1. *Synthesis of acenaphthylene-1,2-diylidene-bis(4-(4-aminophenoxy)aniline) (BIANODA) (Figure S12)*

(8.2 mmol, 1.49 g) Acenaphthenequinone, was stirred under reflux conditions in toluene under N<sub>2</sub> atmosphere till soluble. (30.0 mmol, 6.30 g) 4,4'-Oxadianiline solution in toluene was then added to the previous solution (a total of 120 mL of toluene) in the schlenk flask. A volume of 0.03 mL of conc. sulfuric acid as reaction catalyst was added dropwise to the flask. The mixture was stirred and refluxed for 5 hours under nitrogen. Afterwards, the reaction mixture was allowed to cool to room temperature to obtain a bright orange precipitate in the bottom. The precipitate was isolated and dried under vacuum for removing any solvent. The obtained dried powder was dissolved in 200 mL ethyl acetate, 400 mL hexane was added, and the mixture was stirred for 30 minutes. This solution was kept in the freezer at -15°C overnight. The precipitated product was filtered and washed with 50 mL cold

hexane, and vacuum-dried overnight. A dried orange-red powder (~60 % yield) was obtained. The diamine was characterised by  $^1\text{H}$  (Figure S13) and  $^{13}\text{C}$  NMR (Figure S14), IR (Figure S15) and mass spectroscopy (Figure S16).  $^1\text{H}$  NMR (400 MHz,  $\text{CDCl}_3$ ):  $\delta$  3.53 (s, 4 H),  $\delta$  (ppm) 6.65 (d, 4 H), 6.93 (d, 4 H), 7.05 (m 8 H), 7.12 (t, 2 H), 7.38 (d, 2 H), 7.95 (d, 2 H). IR (neat)  $\nu$  ( $\text{cm}^{-1}$ ) 3490 ( $-\text{NH}_2$ ), 1495 ( $\text{C}=\text{N}$ ), 1290 ( $\text{C}=\text{C}$ ), 1110 ( $\text{C}-\text{N}$ ).

#### 4.2. *Electropolymerisation of BIANODA*

Electropolymerisation of BIANODA was carried out in 0.1M  $\text{LiClO}_4$  in MeCN, with  $\text{Ag}/\text{Ag}^+$  as reference electrode, Pt wire as counter electrode and Pt plate as working electrode. 10 mg of the monomer solution in 100 mL MeCN was used for this purpose. The obtained product was characterised by NMR, IR and UV-Vis spectroscopy.

#### 4.3. *Electrochemical studies*

For all electrochemical studies, commercial  $\text{LiMn}_x\text{Ni}_y\text{Co}_z\text{O}_2$  ( $x=y=z=1/3$ ) electrodes were obtained from Piotrek, Japan, having high weight loading of 10 mg (total weight) per  $\text{cm}^2$  and 1.5  $\text{mAh}/\text{cm}^2$  capacity grade coated on aluminium metal current collector. All the reported capacities are with respect to total electrode weight and not active material weight. 1M  $\text{LiPF}_6$  in 1:1 EC:DEC (Sigma Aldrich) was used as the electrolyte. Appropriate amount of as synthesised and vacuum dried BIANODA was added to commercial  $\text{LiPF}_6$  electrolyte for additive studies. For battery tests, 2025-size coin cells were employed by assembling commercially obtained cathode and Li metal (Honjo metals) as the counter electrode in a cathodic half-cell set up with a polypropylene separator (25 mm, Celgard 2500). The cells were assembled inside an argon-filled glovebox to avoid moisture contamination (UNICO UN-650F,  $\text{H}_2\text{O}$  and  $\text{O}_2$  content  $<0.1$  ppm). The battery charge/discharge tests were performed using a battery cycler (HJ-SD8, Hokuto Denko) at room temperature ( $25^\circ\text{C}$ ). All the other electrochemical techniques described below were performed on a VSP potentiostat (BioLogic) electrochemical analyzer/workstation. Dynamic Electrochemical Impedance

Spectroscopy (DEIS) measurements were performed for the cells after 100 charge discharge cycles over a frequency range from 100 kHz to 10 MHz with a sinus amplitude of 10 mV. Cyclic voltammetry (CV) scans were carried out between OCP and 5V vs Li at a constant rate of 0.1 mVs<sup>-1</sup> to determine the electrochemical behaviour.

#### 4.4. *Material Characterisation*

A Perkin Elmer spectrum 100 FT-IR spectrometer was used to record IR spectra. The spectra were collected using 10 scans with a resolution of 2 cm<sup>-1</sup> in the ATR mode. <sup>1</sup>H and <sup>13</sup>C NMR spectra were obtained with a Bruker Avance II 400 MHz spectrometer. Chemical shifts were reported in ppm using the signals corresponding to the residual protons of the indicated deuterated solvent as an internal standard. Raman studies were conducted on a T64000, HORIBA-JY instrument with 532 nm Nd:YAG laser at 10 mW power and 1800 gr/min. XPS measurements were performed on an AXIS-ULTRA DLD, Shimadzu/Kratos instrument with the sample being coated on a carbon tape. SEM images were obtained on a Hitachi S-4500 FESEM instrument at 1kV acceleration.

### **Supporting Information**

Supporting information available, Figures S1-S13.

### **Author Information**

Corresponding author: [matsumi@jaist.ac.jp](mailto:matsumi@jaist.ac.jp)

**Present Address**

✉ Laboratory of Analysis and Architecture of Systems, CNRS, 7 Avenue Colonel Roche, 31400, Toulouse, France.

‡ Centre for Fuel Cell Technology, International Advanced Research Centre for Powder Metallurgy, Phase I - 2nd Floor, IITM Research Park, Taramani, Chennai 600113, India.

**Competing interests**

The authors declare no competing financial interests.

**Acknowledgement**

S.G.P acknowledges Ministry of Education, Culture, Sports, Science and Technology (MEXT), Japan and JST-MIRAI for financial assistance. We also acknowledge The Center for Nano Materials and Technology (CNMT), in Japan Advanced Institute of Science and Technology, (JAIST) for providing characterization facility.

## References

- 1 F. Wu and G. Yushin, *Energy Environ. Sci.*, 2017, **10**, 435–459.
- 2 S.-T. Myung, F. Maglia, K.-J. Park, C. S. Yoon, P. Lamp, S.-J. Kim and Y.-K. Sun, *ACS Energy Lett.*, 2017, **2**, 196–223.
- 3 M. Gauthier, T. J. Carney, A. Grimaud, L. Giordano, N. Pour, H.-H. Chang, D. P. Fenning, S. F. Lux, O. Paschos, C. Bauer, F. Maglia, S. Lupart, P. Lamp and Y. Shao-Horn, *J. Phys. Chem. Lett.*, 2015, **6**, 4653–4672.
- 4 M. M. Doeff, in *Batteries for Sustainability*, ed. R. A. Meyers, Springer New York, New York, NY, 2013, vol. 10, pp. 5–49.
- 5 D. Aurbach, K. Gamolsky, B. Markovsky, G. Salitra, Y. Gofer, U. Heider, R. Oesten and M. Schmidt, *J. Electrochem. Soc.*, 2000, **147**, 1322.
- 6 M. Stich, M. Göttlinger, M. Kurniawan, U. Schmidt and A. Bund, *J. Phys. Chem. C*, 2018, **122**, 8836–8842.
- 7 F. Lin, I. M. Markus, D. Nordlund, T. Weng, M. D. Asta, H. L. Xin and M. M. Doeff, *Nat. Commun.*, 2014, **5**, 1–9.
- 8 J. Han, S. J. Lee, J. Lee, J. Kim, K. T. Lee and N. Choi, *ACS Appl. Mater. Interfaces*, 2015, **7**, 8319–8329.
- 9 C. Xu, S. Renault, M. Ebadi, Z. Wang, E. Björklund, D. Guyomard, D. Brandell, K. Edström and T. Gustafsson, *Chem. Mater.*, 2017, **29**, 2254–2263.
- 10 H. Lee, T. Han, K. Y. Cho, M. Ryou and Y. M. Lee, *ACS Appl. Mater. Interfaces*, 2016, **8**, 21366–21372.
- 11 L. Wang, Y. Ma, Q. Li, Z. Zhou and X. Cheng, *J. Power Sources*, 2017, **361**, 227–236.
- 12 C. Wang, L. Yu, W. Fan, J. Liu, L. Ouyang, L. Yang and M. Zhu, *ACS Appl. Mater. Interfaces*, 2017, **9**, 9630–9639.
- 13 R. Zhou, J. Huang, S. Lai, J. Li, F. Wang, Z. Chen, W. Lin, C. Li, J. Wang and J. Zhao,

- Sustain. Energy Fuels*, 2018, **2**, 1481–1490.
- 14 W. Huang, L. Xing, Y. Wang, M. Xu, W. Li, F. Xie and S. Xia, *J. Power Sources*, 2014, **267**, 560–565.
- 15 X. Dai, L. Wang, J. Xu, Y. Wang, A. Zhou and J. Li, *ACS Appl. Mater. Interfaces*, 2014, **4**, 15853–15859.
- 16 G.-H. Kim, S.-T. Myung, H. J. Bang, J. Prakash and Y.-K. Sun, *Electrochem. Solid-State Lett.*, 2004, **7**, A477.
- 17 B. Yoon, S. Jung, A. S. Cavanagh, L. A. Riley, S. Kang, A. C. Dillon, M. D. Groner, S. M. George and S. Lee, *Adv. Mater.*, 2010, **22**, 2172–2176.
- 18 U. El-Ayaan and A. a-M. Abdel-Aziz, *Eur. J. Med. Chem.*, 2005, **40**, 1214–1221.
- 19 N. J. Hill, I. Vargas-baca and A. H. Cowley, *Dalt. Trans.*, 2009, **9226**, 213–384.
- 20 Y. H. Budnikova, V. V Khrizanforova, I. L. Fedushkin, A. A. Karasik, V. V Khrizanforova, I. L. Fedushkin and A. A. Karasik, *Phosphorus, Sulfur, and Silicon*, 2016, **191**, 1644–1645.
- 21 I. L. Fedushkin, A. A. Skatova, V. A. Chudakova and G. K. Fukin, *Angew. Chem Int. Ed.*, 2003, **42**, 3294–3298.
- 22 K. Hasan and E. Zysman-Colman, *J. Phys. Org. Chem.*, 2013, **26**, 274–279.
- 23 A. Jacobi von Wangelin, D. Schaarschmidt, M. Villa, D. Miesel, A. Hildebrandt and F. Ragaini, *ChemCatChem*, 2017, **9**, 3203–3209.
- 24 Y. Choi, University of Waterloo, 2011.
- 25 M. Ue, Y. Sasaki, Y. Tanaka and M. Morita, in *Electrolytes for Lithium and Lithium-Ion Batteries*, Springer Science, 2014, pp. 93–162.
- 26 A. M. Haregewoin, A. S. Wotango and B.-J. Hwang, *Energy Environ. Sci. Energy Environ. Sci.*, 2016, **9**, 1955–1988.
- 27 K. M. Shaju, G. V. Subba Rao and B. V. R. Chowdari, *Electrochim. Acta*, 2002, **48**,

- 145–151.
- 28 P. Hou, J. Yin, M. Ding, J. Huang and X. Xu, *Small*, 2017, **13**, 1–29.
- 29 K. S. Smaran, P. Joshi, R. Vedarajan and N. Matsumi, *ChemElectroChem*, 2015, **2**, 1913–1916.
- 30 J. Huang, H. Ge, Z. Li and J. Zhang, *Electrochim. Acta*, 2015, **176**, 311–320.
- 31 J. Huang, Z. Li and J. Zhang, *J. Power Sources*, 2015, **273**, 1098–1102.
- 32 M. Itagaki, N. Kobari, S. Yotsuda, K. Watanabe, S. Kinoshita and M. Ue, *J. Power Sources*, 2005, **148**, 78–84.
- 33 M. Itagaki, N. Kobari, S. Yotsuda, K. Watanabe, S. Kinoshita and M. Ue, *J. Power Sources*, 2004, **135**, 255–261.
- 34 S. S. Zhang, K. Xu and T. R. Jow, *Electrochim. Acta*, 2006, **51**, 1636–1640.
- 35 K. Chung and W. Kim, *J. Ind. Eng. Chem.*, 2004, **10**, 290–294.
- 36 S. G. Patnaik, R. Vedarajan and N. Matsumi, *J. Mater. Chem. A*, 2017, **5**, 17909–17919.
- 37 J. Huang, Z. Li, B. Y. Liaw and J. Zhang, *J. Power Sources*, 2016, **309**, 82–98.
- 38 X. G. Li, M. R. Huang, W. Duan and Y. L. Yang, *Chem. Rev.*, 2002, **102**, 2925–3030.
- 39 F. A. Asswadi, U. S. Yousef, A. S. Hathoot, M. Abdel Azzem and A. Galal, *Arab. J. Chem.*, 2015, **8**, 433–441.
- 40 M. Wang, H. Zhang, C. Wang, X. Hu and G. Wang, *Electrochim. Acta*, 2013, **91**, 144–151.

## Table and Figure Captions

Scheme 1. Structure, general framework and mode of action of BIAN based additive for high voltage cathodes

Figure 1. Comparison of energy levels of BIANODA with various common carbonate solvents (table), DFT optimised structure of EC (a) and DFT optimised structure of BIANODA (b)

Figure 2. CVs with BIANODA (2mg/ml) (a) and control (b) cell in cathodic half-cell set up (MNC cathode in 1M LiPF<sub>6</sub> in EC: DEC w.r.t Li/Li<sup>+</sup>)

Figure 3. Comparison of charge discharge performance with and without BIANODA ( 2mg /ml) at room temperature in potential range (a) 3.0 – 4.5 V and (b) 3.0-4.8 V vs in cathodic half-cell set up (MNC cathode in 1M LiPF<sub>6</sub> in EC: DEC w.r.t Li/Li<sup>+</sup>)

Figure 4. Comparison of rate performance with and without BIANODA ( 2mg /ml) at room temperature in potential range (a) 3.0 – 4.5 V vs in cathodic half-cell set up (MNC cathode in 1M LiPF<sub>6</sub> in EC: DEC w.r.t Li/Li<sup>+</sup>)

Figure 5. DEIS studies during discharge for cell with (a) BIANODA and (b) control

Figure 6. Equivalent circuit used (a) and (b) comparison of R<sub>CEI</sub> of cells with and without additives at different potentials during discharge, from circuit fitting studies

Figure 7. Comparison of morphology of the pristine cathode surface, surface after storing in electrolyte with BIANODA after storing in electrolyte without any additive

Figure 8. Impedance response upon storage with BIANODA (a) and control (b)

Figure 9. XPS spectra for O 1s of (a) pristine cathode, (b) cathode surface after cycling without additive and (c) cathode surface after cycling with additive

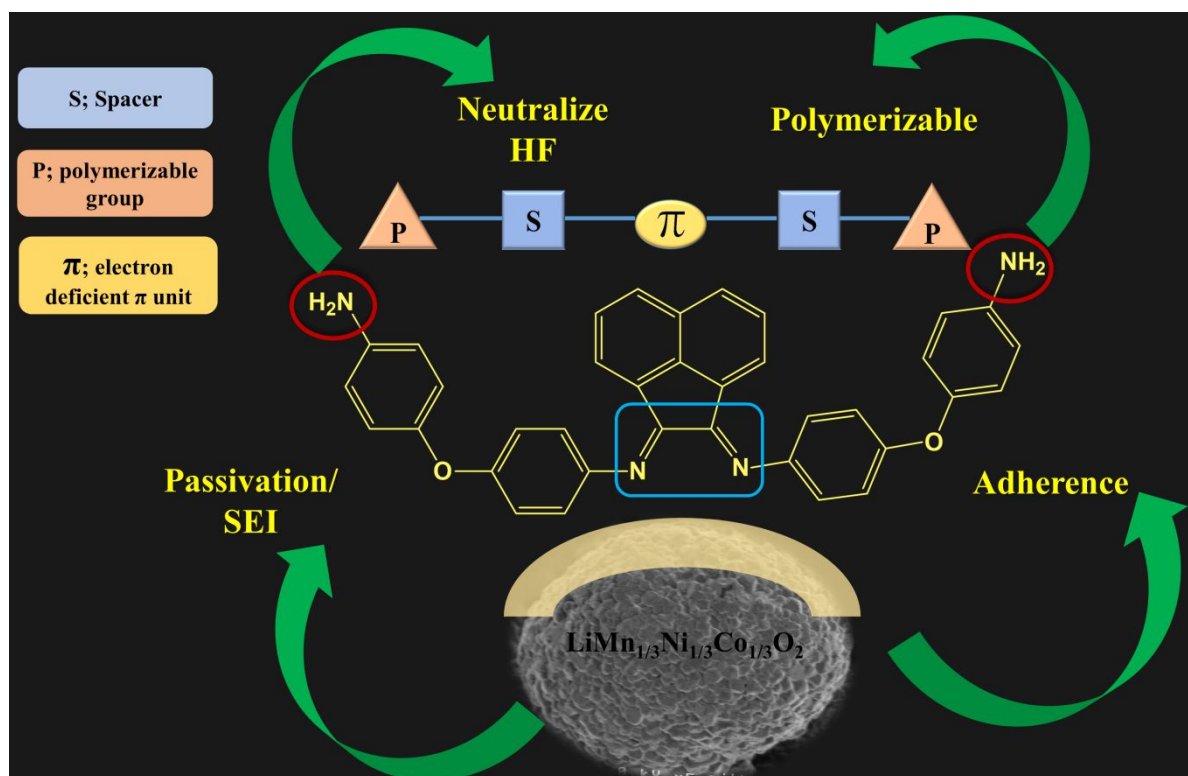
Figure 10. XPS spectra for P 2p of (a) cathode surface after cycling without additive and (b) cathode surface after cycling with additive

Figure 11. XPS spectra for F 1s of (a) pristine cathode, (b) cathode surface after cycling without additive and (c) cathode surface after cycling with additive

Figure 12. Possible scheme of electropolymerisation of BIANODA

Figure 13. Schematic showing possible site for HF neutralization

Figure 14. Schematic showing hopping mechanism of Li<sup>+</sup> through electropolymerised framework of BIANODA



Scheme 1. Structure, general framework and mode of action of BIAN based additive for high voltage cathodes

Material	HOMO (eV)	LUMO (eV)
EC	-12.90	1.74
EMC	-13.33	1.40
DMC	-12.85	1.88
<b>BIANODA</b>	<b>-4.71</b>	<b>-2.06</b>

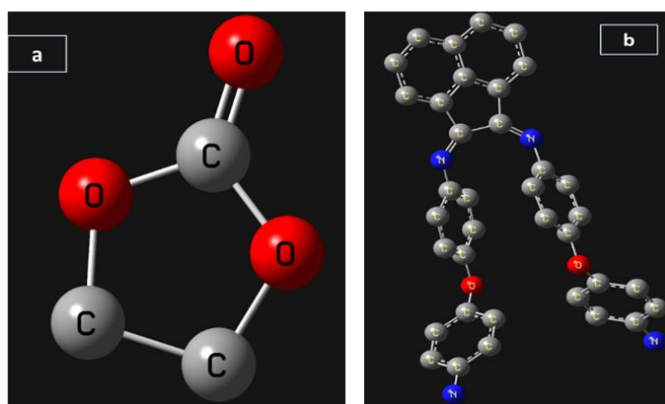


Figure 1. Comparison of energy levels of BIANODA with various common carbonate solvents (table), DFT optimised structure of EC (a) and DFT optimised structure of BIANODA (b)

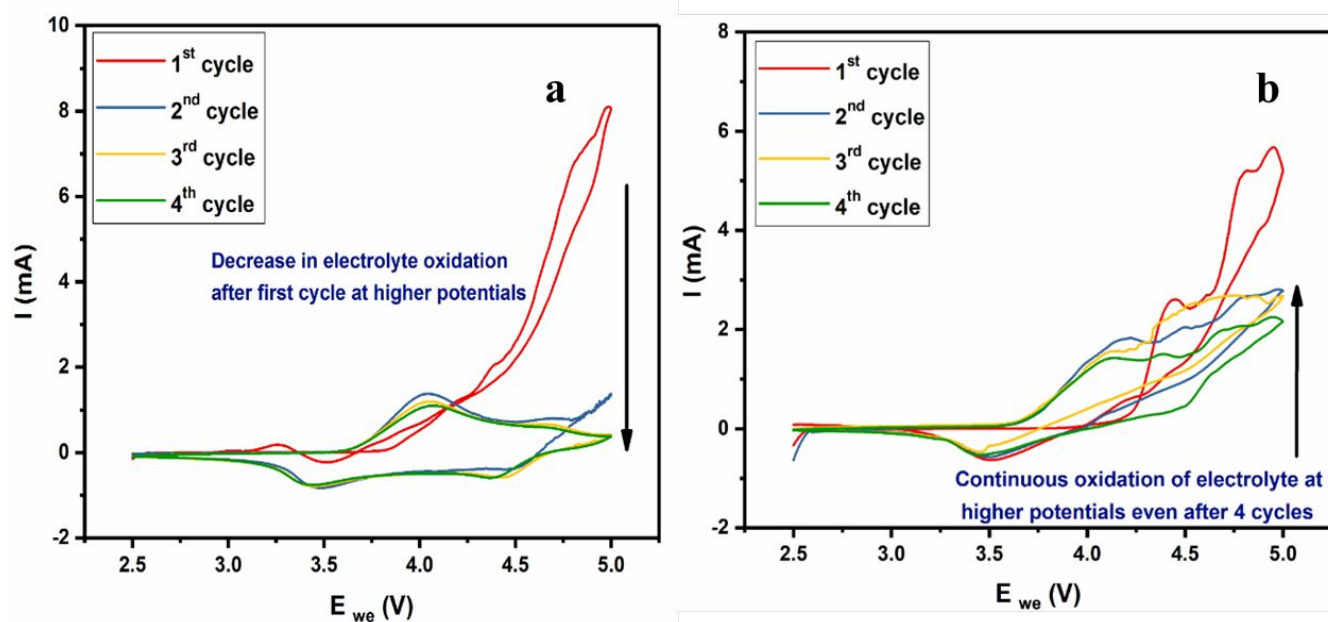


Figure 2. CVs with BIANODA (2mg/ml) (a) and control (b) cell in cathodic half-cell set up (MNC cathode in 1M LiPF<sub>6</sub> in EC: DEC w.r.t Li/Li<sup>+</sup>)

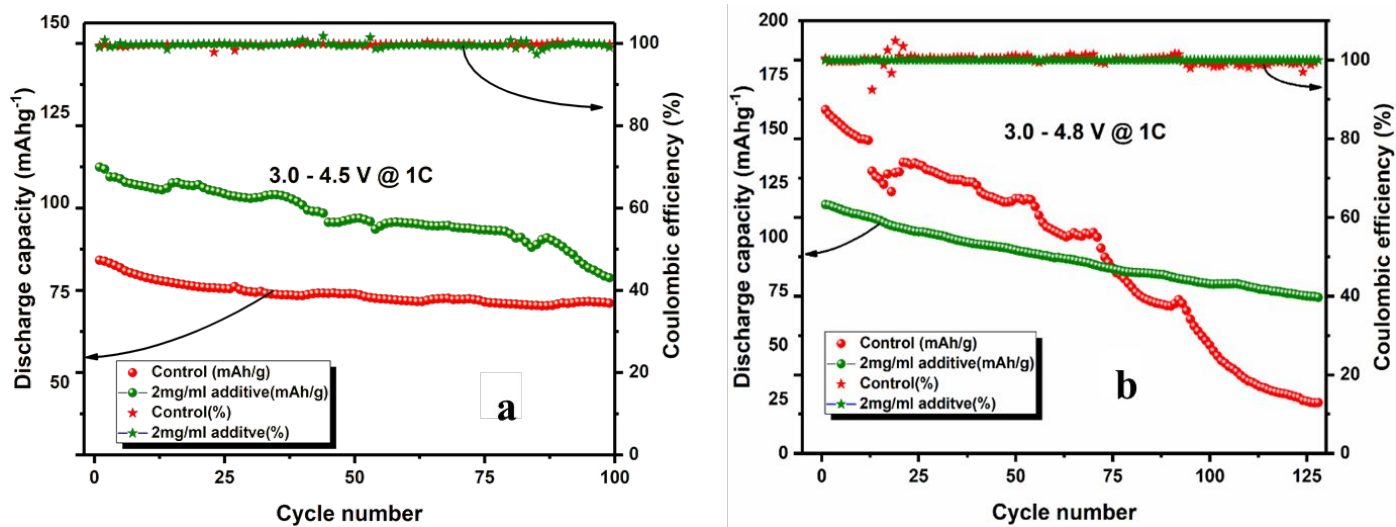


Figure 3. Comparison of charge discharge performance with and without BIANODA ( 2mg /ml) at room temperature in potential range (a) 3.0 – 4.5 V and (b) 3.0-4.8 V vs in cathodic half-cell set up (MNC cathode in 1M LiPF<sub>6</sub> in EC: DEC w.r.t Li/Li<sup>+</sup>)

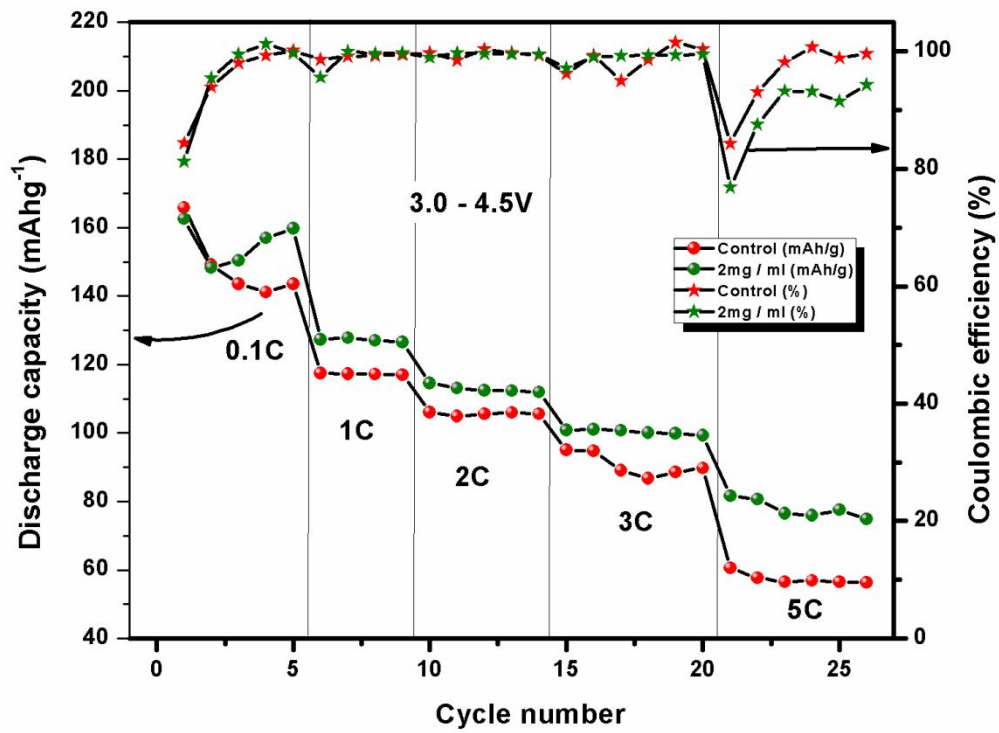


Figure 4. Comparison of rate performance with and without BIANODA (2 mg/ml) at room temperature in potential range (a) 3.0 – 4.5 V vs in cathodic half-cell set up (MNC cathode in 1M LiPF<sub>6</sub> in EC: DEC w.r.t Li/Li<sup>+</sup>)

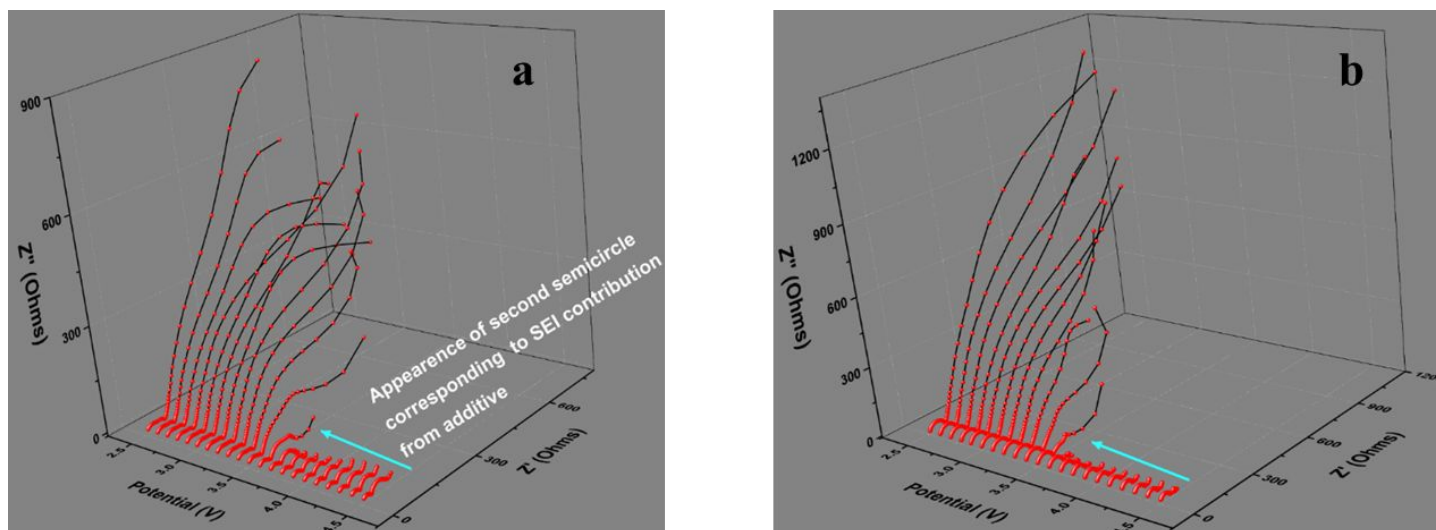
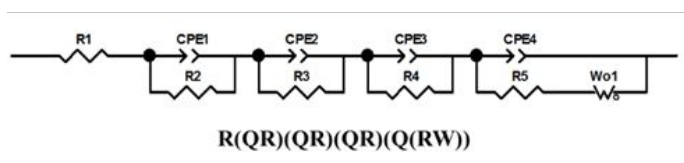
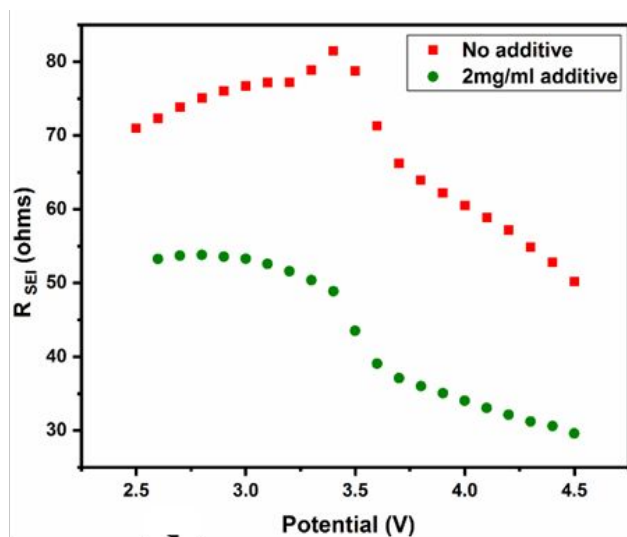


Figure 5. DEIS studies during discharge for cell with (a) BIANODA and (b) control

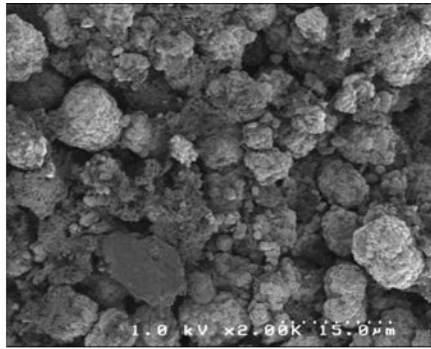
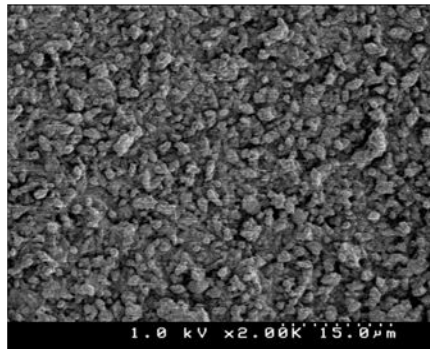
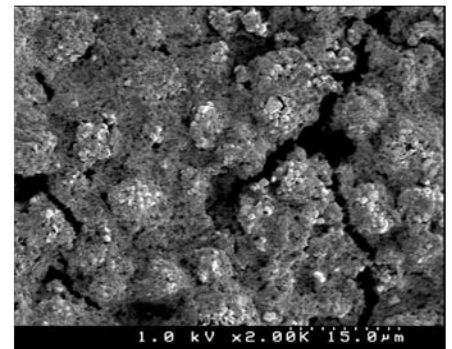
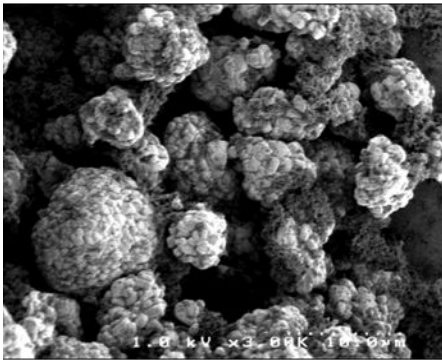
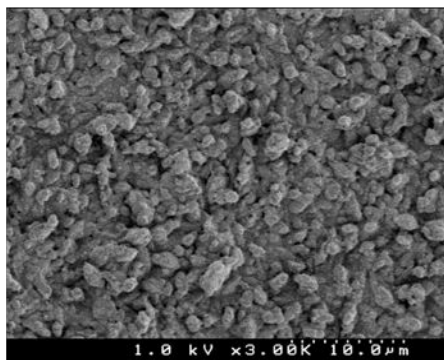
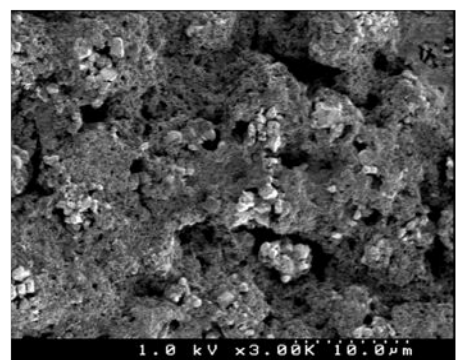
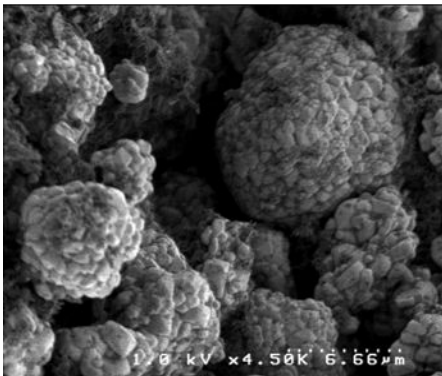
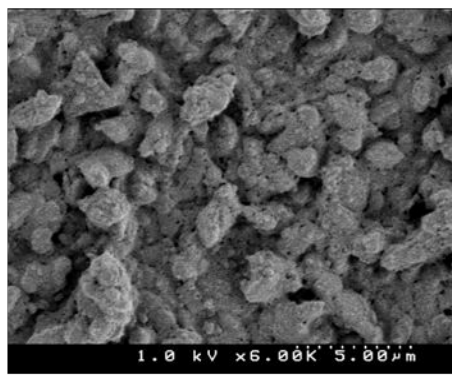
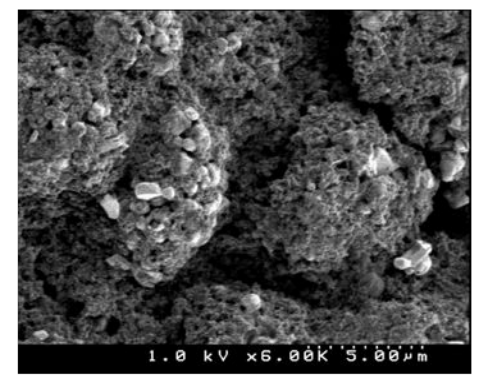


**a**



**b**

Figure 6. Equivalent circuit used (a) and (b) comparison of  $R_{SEI}$  of cells with and without additives at different potentials during discharge, from circuit fitting studies

**Pristine cathode****After storage – no additive****After storage – with BIANODA****Pristine cathode****After storage – no additive****After storage – with BIANODA****Pristine cathode****After storage – no additive****After storage – with BIANODA**

**Figure 7. Comparison of morphology of the pristine cathode surface, surface after storing in electrolyte with BIANODA after storing in electrolyte without any additive**

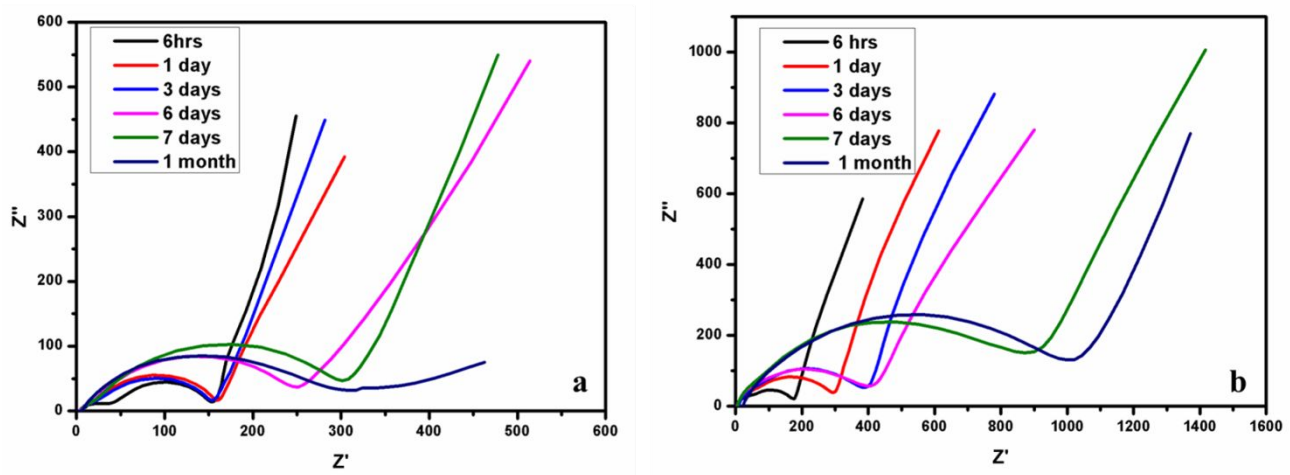


Figure 8. Impedance response upon storage with BIANODA (a) and control (b)

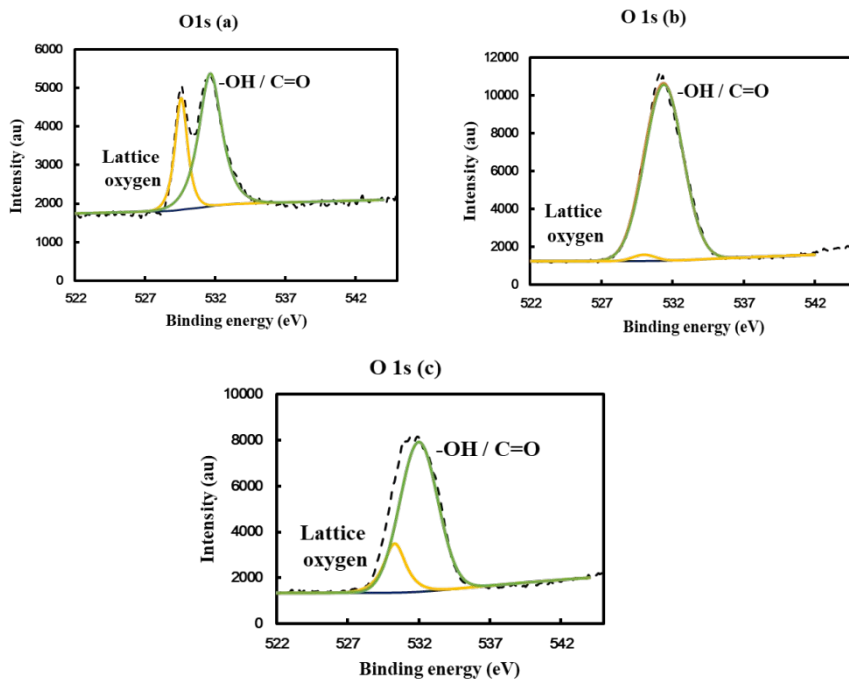


Figure 9. XPS spectra for O 1s of (a) pristine cathode, (b) cathode surface after cycling without additive and (c) cathode surface after cycling with additive

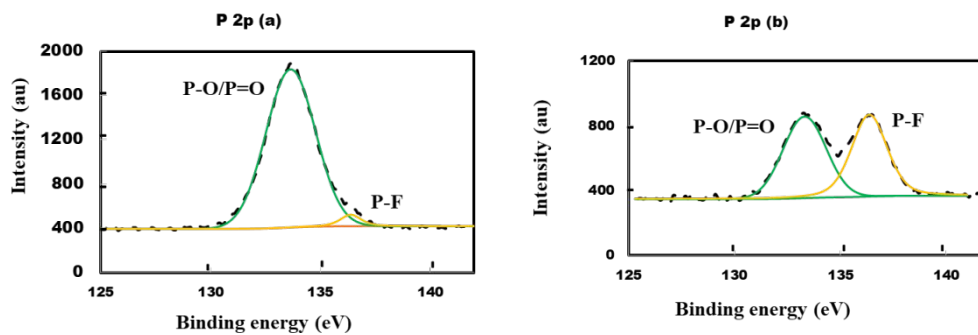


Figure 10. XPS spectra for P 2p of (a) cathode surface after cycling without additive and (b) cathode surface after cycling with additive

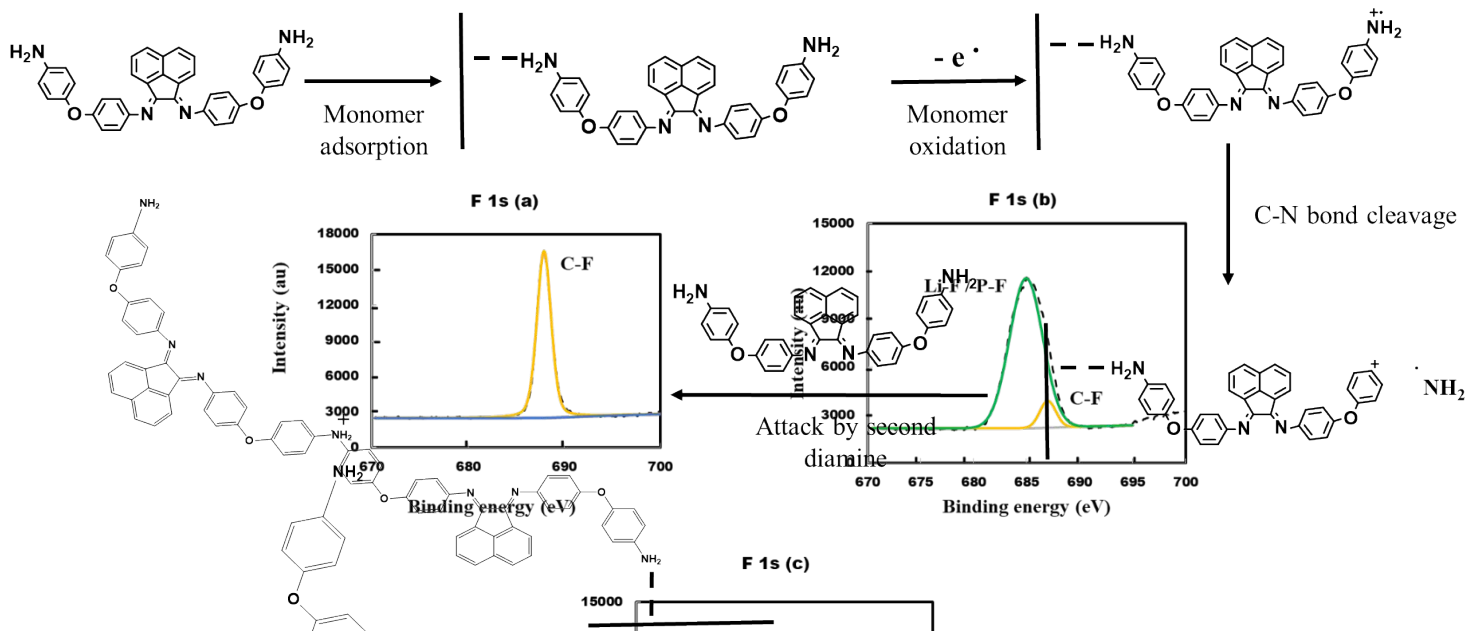


Figure 11. Possible scheme of electropolymerisation of BIANODA

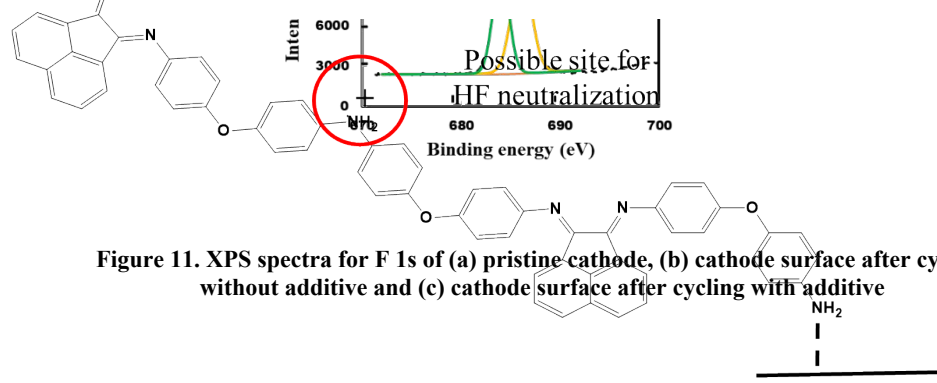


Figure 11. XPS spectra for F 1s of (a) pristine cathode, (b) cathode surface after cycling without additive and (c) cathode surface after cycling with additive

Figure 13. Schematic showing possible site for HF neutralization

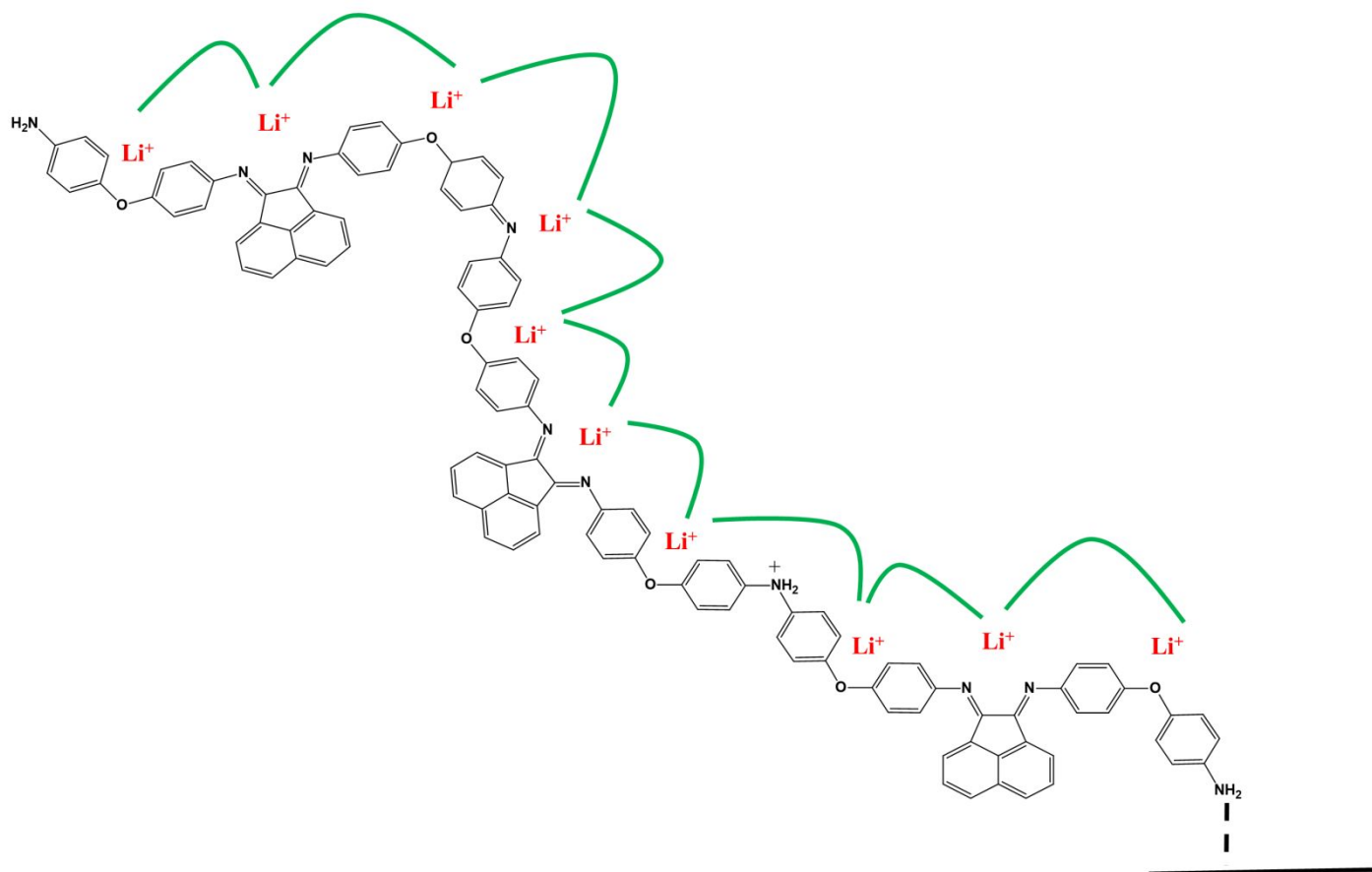
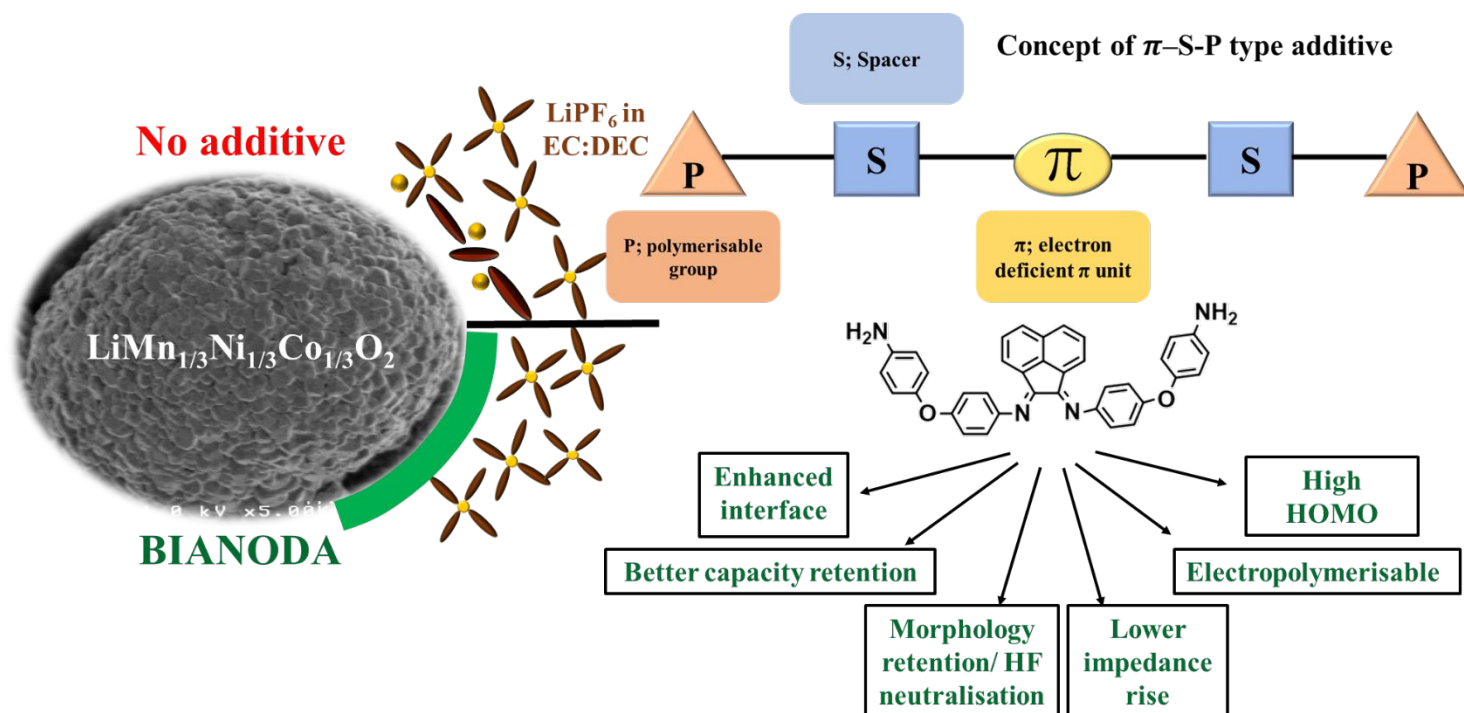


Figure 14. Schematic showing hopping mechanism of  $\text{Li}^+$  through electropolymerised framework of BIANODA



Graphical Abstract